Atomic-scale modelling of kinetic processes occurring during silicon oxidation

2005 J. Phys.: Condens. Matter 17 S2051

(http://iopscience.iop.org/0953-8984/17/21/002)

INSTITUTE OF PHYSICS PUBLISHING JOURNAL OF PHYSICS: CONDENSED MATTER

J. Phys.: Condens. Matter **17** (2005) S2051–S2063 doi:10.1088/0953-8984/17/21/002

Atomic-scale modelling of kinetic processes occurring during silicon oxidation

Angelo Bongiorno[1] **and Alfredo Pasquarello**

Institut de Théorie des Phénomènes Physiques (ITP), Ecole Polytechnique Fédérale de Lausanne (EPFL), CH-1015 Lausanne, Switzerland
and
Institut Romand de Recherche Numérique en Physique des Matériaux (IRRMA),
CH-1015 Lausanne, Switzerland

E-mail: Angelo.Bongiorno@physics.gatech.edu and Alfredo.Pasquarello@epfl.ch

Received 18 November 2004, in final form 18 November 2004
Published 13 May 2005
Online at stacks.iop.org/JPhysCM/17/S2051

Abstract
We model the fundamental kinetic processes occurring during silicon oxidation at the atomic scale. We first focus on the diffusion of the neutral O_2 molecule through the oxide layer. By combining *ab initio* and classical simulations, we derive a statistical description for the O_2 potential energy landscape in the oxide. Statistical distributions are then mapped onto lattice models to investigate the O_2 diffusive process in the bulk oxide and across an oxide layer at the Si(100)–SiO_2 interface. We find that the diffusion of O_2 is a percolative process, critically influenced by both energetical and geometrical features of the potential energy landscape. At the interface, the occurrence of a thin densified oxide layer in contact with the substrate limits percolative phenomena and causes the O_2 diffusion rate to drop below its value for ordinary amorphous SiO_2. Then, we use first-principles calculations to address the kinetic processes occurring in the proximity of the Si(100)–SiO_2 interface. We first focus on the energetics of negatively charged oxygen species in the oxide, and on the diffusive and dissociative properties of the charged molecular species. We find that negatively charged oxygen species incorporate in the oxide at Si sites, giving rise to additional Si–O bonds and important network distortions. Finally, we focus on the oxidation reaction at the Si(100)–SiO_2 interface. We find that the O_2 oxidation reaction occurs by crossing small energy barriers, regardless of the spin or charge state of the molecular species. Our findings are consistent with kinetics pictures of the silicon oxidation process entirely based on diffusive phenomena.

---

[1] Present address: Georgia Institute of Technology, School of Physics, 837 State Street, Atlanta, GA 30332-0430, USA.

1. Introduction

Gate dielectrics in current Si-based electronic devices consist of thermally grown silicon dioxide (SiO_2) films with thicknesses of about 2 nm [1–5]. In this regime, the tuning of device performance depends on the ability of controlling the oxide growth at the atomic scale. Further progress therefore requires the understanding of the mechanisms responsible for the growth of ultrathin SiO_2 films.

Since the work of Deal and Grove [6], the silicon oxidation process is commonly depicted as follows: an O_2 molecule at the vacuum/oxide surface enters into the pre-existing oxide layer, then diffuses through the disordered oxide network toward the Si substrate, and finally reacts at the Si(100)–SiO_2 interface [6]. The Deal–Grove model successfully reproduces a large variety of kinetic data on the growth of thick oxide films [6–9]. This regime is governed by the O_2 diffusion through the oxide layer [6], and its description meets nowadays broad consensus approval. Indeed, kinetic data [6], experiments on O_2 permeation through silica membranes [10], and isotopic tracer experiments on ^{16}O–^{18}O sequentially oxidized films [11, 12] all consistently confirm the Deal–Grove description of the oxygen diffusion process. In contrast, the growth kinetics of thin oxide films is far less understood. According to the Deal–Grove model, this regime is dominated by the oxidation reaction at the Si(100)–SiO_2 interface [6, 13]. However, the Deal–Grove model fails in describing the oxidation kinetics of thin-film oxides [6, 9, 14]. Moreover, isotope depth analysis experiments on ultrathin oxide films show overlapping depth profiles of both ^{16}O and ^{18}O isotopes during the first 20–25 Å of oxide growth [11]. More recently, oxygen exchange processes have also been found to occur at the Si–SiO_2 interface [15, 16]. These experimental findings suggest that, for very thin films, oxygen exchange processes occur throughout the film, in contrast with the Deal–Grove model. To account for the thin-film regime, a variety of alternative kinetics schemes have been proposed, based on different underlying mechanisms [14, 17–24]. However, no direct observations can at present distinguish among these modelling schemes, their purpose remaining limited to reproducing the kinetics of the silicon oxidation process.

Theoretical investigations based on density functional theory have been demonstrated to be particularly suitable for providing insight into the atomic processes occurring during silicon oxidation [25–28]. Many studies have focused on the relative energetics of oxygen species in SiO_2 [29–35]. In agreement with experiments [11, 12, 10], these investigations identify the O_2 molecule as the oxidizing species during silicon oxidation. The diffusive properties of the O_2 molecule have been addressed for both α-quartz [33] and amorphous SiO_2 [36, 35]. Very recently, O_2 diffusion in the oxide has been fully characterized by adopting a multiscale modelling approach [37, 38]. The calculated activation energy for diffusion results in excellent agreement with experimental data [10, 6]. The energetics of negatively charged oxygen species in SiO_2 have also been addressed [30, 36, 39]. Furthermore, recent investigations have provided insight into the oxidation reaction at the Si(100)–SiO_2 interface [40–42].

The present paper reports on the current atomic-scale understanding of the kinetics process occurring during silicon oxidation [37, 43, 38, 42]. We first address the process of O_2 diffusion across the oxide layer. In the case of a thin oxide film, we investigate the effect of a denser interfacial oxide [44, 45] on the O_2 diffusion (section 2). Then, we focus on the properties of negatively charged oxygen species in the oxide (section 3). We address their energetic stability with respect to the neutral O_2 molecule, as well as the diffusion and dissociation properties. Finally, we address the oxidation reaction at the Si(100)–SiO_2 interface (section 4). We conclude by discussing the kinetics picture emerging from our findings (section 5).

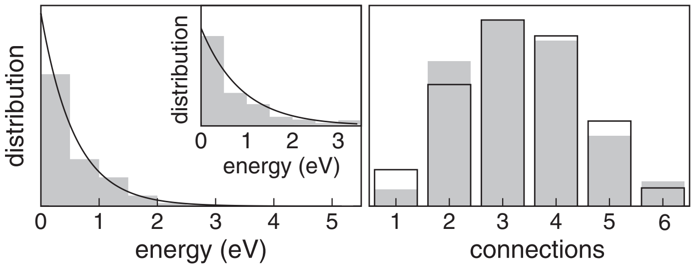

Figure 1. Energy distributions of minima (left panel) and lowest barriers (inset), and the distribution of connections between nearest neighbour equilibrium sites (right panel) for the interstitial O_2 molecule in a-SiO_2. Histograms relate to model structures of the oxide examined within the classical scheme. Exponential decaying functions (solid curves) and a sixth-degree binomial distribution with a coefficient of 0.55 (open histogram) are found to reproduce well the data extracted from the atomistic model structures of the oxide (filled histogram).

2. O_2 diffusion across the oxide layer

Recently, we used a multiscale modelling approach for studying the process of O_2 diffusion through the oxide layer during silicon oxidation [37, 43, 38]. We first addressed the diffusion process in a region well separated from the Si(100)–SiO_2 interface, where the oxide acquires the same properties as amorphous SiO_2 [37]. Then, we extended our study to the case of O_2 diffusion across an oxide layer at the interface [43, 38]. We here report on the main results obtained in these studies [37, 43, 38].

Our multiscale approach consisted in employing a hierarchy of different methodologies and schemes [37]. We first used first-principles calculations to investigate the energetics of the O_2 molecule and of the peroxyl and ozonyl linkages in amorphous SiO_2. This study showed that the O_2 molecule is the most stable oxygen species in the oxide and that its local minima correspond to interstitials of the oxide network. To explore the energetics of the O_2 molecule on a larger spatial scale, we then resorted to a classical scheme consisting of a combination of intra-SiO_2 [46] and O_2–SiO_2 interactions [37, 38]. This simplified scheme was used to derive a complete picture of the O_2 potential energy landscape in both ordinary (2.2 g cm^{-3}) and densified (2.4 g cm^{-3}) amorphous SiO_2. In particular, we generated a large set of model structures for the oxide at both densities. Hence, for each model structure we extracted the energy and location of the O_2 minima and saddle points. The full set of data allowed us to achieve a statistical description of the energetical and topological properties of the O_2 potential energy landscape in the oxide.

In ordinary amorphous SiO_2 (a-SiO_2), the average distance between nearest neighbouring O_2 minima is about 5.7 Å and their energies appear distributed according to an exponential function with a decay constant of 0.6 eV (figure 1, left panel). In densified amorphous SiO_2 (d-SiO_2), the average interstitial volume is smaller [38]. This is consistent with both the reduction of the average distance between O_2 minima (5.3 Å) and the increase of the mean value of the corresponding energy distribution (figure 2, left panel) [38]. Neighbouring O_2 minima in the disordered oxide share an asymmetric barrier. For both a-SiO_2 and d-SiO_2, we found that the energy distributions associated with the low-barrier side are well described by exponential functions with decay constants of 0.9 and 1.7 eV, respectively (insets in figures 1 and 2). The locations of the transition states define the connectivity of the network of local minima for O_2 diffusion. Our analysis shows that the distribution of connections in a-SiO_2 is well described by a binomial distribution of degree $N = 6$ and probability $p = 0.55$ (figure 1, right panel). Similarly, for d-SiO_2, we found $N = 12$ and $p = 0.34$ (figure 2, right panel).

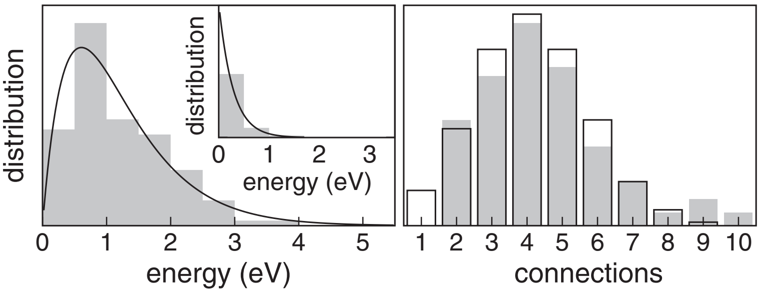

Figure 2. Energy distributions of minima (left panel) and lowest barriers (inset), and the distribution of connections between nearest neighbour equilibrium sites in amorphous SiO_2 at a density of 2.4 g cm^{-3}. Histograms relate to actual model structures of the oxide, while solid lines correspond to fitted continuous distributions. A twelfth-degree binomial distribution with a coefficient of 0.34 is used to describe the distribution of connections.

The study of the O_2 diffusion process in the oxide requires spanning large scales of length and time. To account for an extended region of the oxide, we reproduced the O_2 potential energy landscape on lattice models by using the energy distributions for minima and transition states, as well as the distribution of connections (figures 1 and 2) [37, 38]. Hence, we studied the long-range O_2 diffusion process by means of extensive Monte Carlo simulations. We first addressed the diffusion process in bulk a-SiO_2 and d-SiO_2 [37, 38]. Diffusion coefficients were estimated at temperatures typically adopted during silicon oxidation (1000–1500 K). In this interval of temperatures, our simulations show a quasi-Arrhenian behaviour with a corresponding effective activation energy of 1.12 and 2.0 eV for a-SiO_2 and d-SiO_2, respectively [37, 38]. These values are consistent with experimental estimates [10, 47]. Our simulations show that the long-range O_2 diffusion process mainly involves the lowest-energy part of the energy landscape, allowing percolation throughout the oxide [37]. Noticeably, the highest energy values visited during the motion are located around the effective activation energy for O_2 diffusion. These values are well below the energy intervals corresponding to peroxyl and ozonyl linkages, indicating that processes of oxygen exchange with the network are unlikely during O_2 diffusion [37, 38]. This result is consistent with the experimental evidence that oxygen exchange processes are not found to occur in the bulk of the oxide during silicon oxidation [12, 48–51, 15, 16].

For very thin oxide films, the experimental growth rates appear anomalously larger than the value predicted by the Deal and Grove model [8, 14]. To better describe kinetic data in the thin-film regime, numerous alternative kinetics models have been advanced [14, 17–24]. Among such models, several kinetics schemes are simply based on the assumption that the oxidation kinetics is fully governed by the diffusion process, with a diffusion rate decreasing with decreasing oxide thickness [14, 24].

We first considered homogeneous oxide layers with ordinary density. Our simulations show that the O_2 diffusion rate across the oxide layer increases with decreasing thickness (figure 1, left panel). This behaviour is related to the percolative nature of the diffusion process. In fact, when the layer thickness drops, the number of low-barrier paths increases, resulting in an increase of the diffusion coefficient. For thick layers, the bulk value is recovered (figure 1, left panel). Then, in accord with x-ray reflectivity experiments [44, 45], we accounted for the occurrence of a 10 Å thick densified oxide layer with a density of 2.4 g cm^{-3} at the Si–SiO_2 interface. The diffusion coefficient for such composite oxide layers is given as a function of oxide thickness in figure 3, right panel. As expected, the diffusion coefficient is now lower than for homogeneous oxide layers. More interestingly, the diffusion coefficient is found to approach from below the bulk limit corresponding to amorphous SiO_2 at ordinary

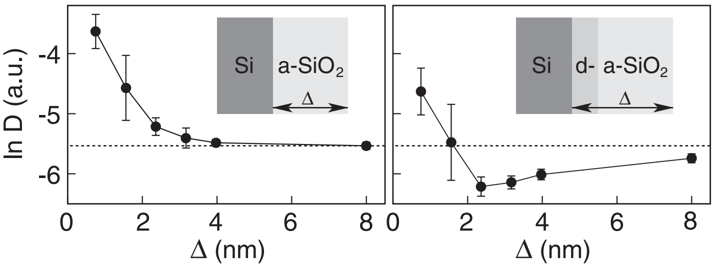

Figure 3. Calculated diffusion coefficients in the direction perpendicular to the plane of the interface for homogeneous (left panel) and nonhomogeneous (right panel) oxide layers of varying thickness. A homogeneous oxide layer has the same properties as a-SiO$_2$ (light band). The nonhomogeneous layers account for the occurrence of a 1 nm thick layer of d-SiO$_2$ (grey band) in contact with the Si substrate (dark band). The horizontal dashed line corresponds to the diffusion coefficient in bulk a-SiO$_2$.

density [43, 38]. The diffusion coefficient lies below the bulk limit for oxide thicknesses down to about 2 nm. This result indicates that the presence of a denser oxide can indeed account for a lower diffusion coefficient during oxidation.

3. Negatively charged oxygen species in a-SiO$_2$

SiO$_2$ is an insulating material. The conduction band and valence band offsets at the Si(100)–SiO$_2$ interface are 3.15 and 4.6 eV, respectively [52]. These high barriers prevent the O$_2$ molecules from charging when they diffuse in the oxide at large distances from the Si substrate. These arguments are supported by experiments which show that oxidation rates of very thick oxide films are unaffected by an external electric field [53–57]. However, close to the Si(100)–SiO$_2$ interface, charge tunnelling becomes much more favourable and charged oxygen species may therefore play a more fundamental role in the oxidation process. To understand the role played by these charged species during the growth of thin films, we investigated their physical properties by using first-principles calculations.

3.1. Energetics of negatively charged oxygen species

To address the energetics of negatively charged atomic and molecular oxygen species in the oxide, either singly or doubly charged, we used first-principles calculations based on density functional theory [58, 59]. In our scheme, the exchange and correlation energy was accounted for within a generalized gradient approximation [60]. A norm-conserving [61] and an ultrasoft [62] pseudopotential were used for Si and O, respectively. Plane-wave cut-offs of 24 and 150 Ryd were used for the wavefunctions and the augmented electron density, respectively [63, 64]. In this framework, we prevented the energy from diverging by using a neutralizing background [65]. The spurious interaction between the uniform background and the net charge in the periodic cell was accounted for by using the monopole–monopole correction [65]:

$$E_{\mathrm{corr}}(n) = \frac{n^2\alpha}{2L\epsilon} \tag{1}$$

where α is the lattice-dependent Madelung constant (for cubic cells, $\alpha = 2.82$ [66]), n is the number of additional or subtracted electrons, ϵ the dielectric constant of the underlying periodic medium, and L the linear size of the cell [65].

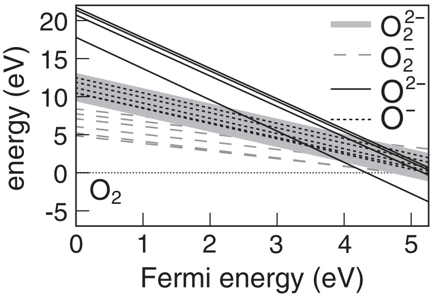

Figure 4. Formation energies for negatively charged oxygen species in amorphous SiO_2 as a function of the Fermi energy in the gap. The calculated energy gap is 5.3 eV. At the top right corner, the species considered with the corresponding legend appears. Energies are referred to that of the O_2 molecule in the vacuum. The neutral O_2 molecule located in large interstitials of a-SiO_2 has similar energies.

For the oxide, we used a model structure of silica containing 24 SiO_2 units [37]. Each species was inserted in several different locations inside the model structure of the oxide. Upon relaxation within our first-principles scheme, the formation energy E_f of the charged oxygen species was estimated according to

$$E_f = E + E_{corr}(n) - E_0 - e_0 - n\mu \qquad (2)$$

where E is the energy of the defected system, E_{corr} the correction term in equation (1), E_0 the energy of the unperturbed SiO_2 network, e_0 the energy of the neutral isolated defect, and μ the electron Fermi energy. The energy of an isolated O_2 molecule was used as the reference for both atomic and molecular species. Hence, the formation energy of an atomic species corresponds to the energy of two identical defects at infinite distance in the oxide. We also note that energies for charged defects depend on the position of the electron Fermi energy μ within the gap. To compare charged and neutral defects, μ is usually referred to the position of the valence band edge e_v in the unperturbed periodic system: $\mu = e_v + \chi + \Delta V$, with χ varying between the valence and the conduction band edges and ΔV being a correction term needed to align the potential of the defected system with that of the bulk. We estimated a ΔV of -0.14 eV and -0.24 eV for the atomic and molecular oxygen species, respectively.

In figure 4, the formation energies of the negatively charged oxygen species are reported as a function of the Fermi energy in the gap (χ) and are compared to the lowest energy for the neutral O_2 molecule in a-SiO_2 [37]. Neutral O_2 remains the most stable species until the Fermi energy reaches a value of about 4.4 eV. Above this value, the negatively charged oxygen species become more stable. Due to the disordered nature of the oxide, the formation energies of the negatively charged species are spread over a wide interval. These intervals overlap for Fermi energies χ between 4.4 and 5.3 eV (figure 4). Hence, on the basis of the present framework, it remains unclear which charged species is most stable in a-SiO_2 for $\chi > 4.4$ eV. Nevertheless, due to the larger slope of E_f with χ, the O^{2-} species appears to be eventually favoured for increasing Fermi energies. The diffusion properties of O^{2-} in α-quartz have been investigated in a recent study [39].

At variance with the neutral O_2 molecule which occupies interstitial positions in the oxide, negatively charged species prefer to incorporate in the SiO_2 network (figure 5). Because of the disordered nature of a-SiO_2, we found several different local minima for each species. However, we observed some general features in the binding properties of the negatively charged O species with the oxide network. O^- incorporates in the oxide network in correspondence with Si atoms which become fivefold coordinated with O. The additional O^- atom constitutes a

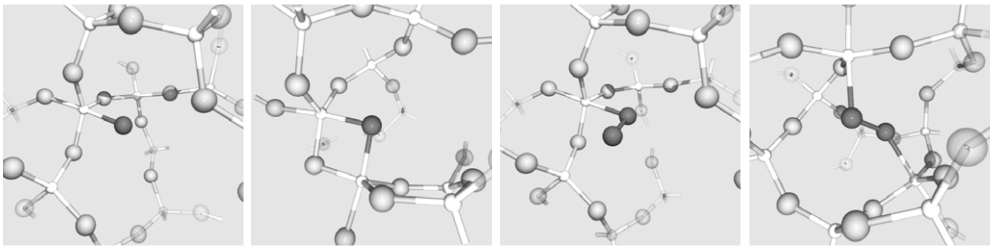

Figure 5. A ball and stick representation of the most common stable configurations of negatively charged oxygen species in amorphous SiO_2. Light (shaded) spheres relate to Si (O) atoms of the oxide network. O atoms belonging to the charged defects are represented by darker spheres. In sequence: O^-, O^{2-}, O_2^-, and O_2^{2-}.

dangling appendix of the oxide network protruding toward the nearest interstitial void. The O^{2-} species behaves similarly, but its lowest-energy configuration is obtained when the O appendix bends toward a neighbour O atom of the network to form a supplementary Si–O bond. The final configuration corresponds to an oxygen double-bridge structure [39] (figure 5). Negatively charged molecular oxygen species tend to incorporate in the network by forming bonds with Si atoms. O_2^- and O_2^{2-} prefer to form one and two Si–O bonds, respectively (figure 5).

With respect to atomic species, negatively charged molecular oxygen species preserve their individuality upon incorporation in the network. For these species, it is therefore possible to investigate how the competition between electronic and strain effects determines the defect energy. Assuming that the excess negative charge is well localized on the molecular oxygen species, we extracted the defect together with its charge from the relaxed system and calculated the energy of the remaining neutral structure, E_{SiO_2}, without allowing for further structural relaxations. Hence, this energy value was used to split the formation energy of negatively charged molecular oxygen species in a-SiO_2 as follows:

$$E_f = [E + E_{corr}(n) - E_{SiO_2} - e_0 - n\mu] + [E_{SiO_2} - E_0] \tag{3}$$

where the first term between squared brackets corresponds to the energy change due to electronic effects (capture of n electrons and consequent binding of the molecular species to the oxide network), while the second one accounts for the strain energy of the oxide network induced by the incorporation of the charged species. The deformation of the molecule is negligible.

We calculated E_{SiO_2} from first principles for various configurations of O_2^- and O_2^{2-} in a-SiO_2. To split the formation energy according to equation (3), we aligned the Fermi energy μ with the Si conduction band edge at the Si(100)–SiO_2 interface, using experimental values of the valence band offset at the interface (4.6 eV) and of the Si band gap (1.1 eV) for its determination. Our calculations show that the electronic part of the formation energy ranges between −2.8 and −3.3 eV for O_2^-, and between −5.0 and −8.5 eV for O_2^{2-}. Instead, the strain energy of the oxide network takes values ranging between 1.5 and 4.7 eV for O_2^-, and varies between 3.8 and 6.3 eV for O_2^{2-}. These results suggest that negatively charged molecular species strongly perturb the oxide network. The oxide deformation energy induced by their incorporation in the network contributes significantly to the formation energy. Moreover, the ranges of values for both the electronic and strain parts of the formation energy suggest that their energy landscape is strongly affected by the disordered nature of the oxide.

3.2. The energy landscape for O_2^- and O_2^{2-} in a-SiO_2

O_2^- and O_2^{2-} significantly bind and deform the oxide network in correspondence with local energy minima (section 3.1). This behaviour contrasts with that of the neutral O_2 molecule

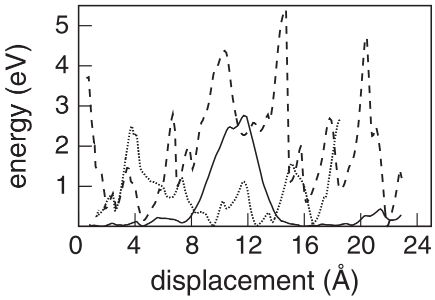

Figure 6. Energy profiles along a diffusion pathway for neutral O_2 (solid), O_2^- (dotted), and O_2^{2-} (dashed), in a model structure of amorphous SiO_2. For each curve, energy is referred to the lowest value attained along the migration pathway.

which finds local minima in interstitials, barely perturbing the surrounding oxide network [37]. We carried out further analysis of the energy landscape by exploring transition states for O_2^- and O_2^{2-} migration in a-SiO_2. To this end, we moved the molecular species along migration pathways by applying an external force. We started from an equilibrium configuration of the charged species in the model structure of the oxide. Then, we introduced an external short-range repulsive potential acting on the centre of mass of the molecule. The strength and the range of this potential were set to increase slowly and gradually with time. During the evolution, the centre of mass of the oxide matrix was kept fixed and the kinetic energy was constantly extracted from the full system by damping the electronic degrees of freedom [67]. In this way, the molecular species was moved through the oxide network without leaving the Born–Oppenheimer energy surface. For the neutral O_2 in a-SiO_2 as described within the classical scheme (section 2), we verified that this method gave the same saddle points as were identified with the activation relaxation technique [68] and a dragging procedure [38].

We generated within a first-principles scheme a diffusion pathway for the O_2, O_2^-, and O_2^{2-} molecules in a model structure of a-SiO_2. Starting from an equilibrium configuration, we moved the molecular species through the disordered oxide for a distance of about 24 Å. As expected, the neutral O_2 molecule was found to diffuse easily through the interstices of the network. Along the migration pathway, the highest transition barrier was encountered when crossing a fivefold ring (figure 6). Because of the percolative nature of the diffusion, these high barriers are usually avoided during diffusion at finite temperature [37]. In contrast with neutral O_2, charged molecular species show more complicated energy profiles along the migration pathways. O_2^- proceeds by sequentially switching the O atom of the molecule which binds with Si atoms of the network. In the case of O_2^{2-}, both atoms of the molecule tend to form bonds with Si atoms of the network. Accordingly, the migration appears to be strongly hindered (figure 6). Indeed, the energy profile corresponding to the migration of O_2^{2-} extends over about twice the range of energies determined for O_2^- (figure 6). These results are consistent with the range of values for the electronic and strain parts of the formation energy, calculated in the previous section for local minima of O_2^- and O_2^{2-}.

3.3. *O_2^- and O_2^{2-} dissociation in a-SiO_2*

The negatively charged molecular species can dissociate into two atomic species. In a-SiO_2, O_2^- can give rise to an O^- ion and a peroxyl linkage while the O_2^{2-} species can dissociate into either two separated O^- or into a O^{2-} and a peroxyl linkage. We addressed the energetics of these reactions by using first-principles calculations. In particular, we evaluated transition barriers using the scheme presented in the previous section. In this case, the external potential stimulates the dissociation. At each step of the procedure, the origin of the spherical repulsive potential is located at the centre of mass of the molecular species. Moreover, it acts independently on each of the O atoms of the molecule.

We considered several equilibrium configurations for both the O_2^- and O_2^{2-} defects in a-SiO_2. Our first-principles calculations show that these negatively charged species dissociate by overcoming energy barriers of 2.4–3.2 and 1.2–1.8 eV for O_2^- and O_2^{2-}, respectively. For both the O_2^- and O_2^{2-} species, the disordered nature of the oxide spreads the energy barriers for dissociation over an interval of about 0.7 eV. Nevertheless, we found an average energy barrier for O_2^{2-} which is approximately half that for O_2^-. This is consistent with the weakening of the O–O bond with the increase of the negative charge carried by the molecule. Indeed, experimental values for the dissociation energy are 5.1 and 4.1 eV for O_2 and O_2^-, respectively [69].

The process of dissociation of O_2^- and O_2^{2-} leads to a couple of neighbouring atomic oxygen defects in a-SiO_2. We found that the products of dissociation are higher in energy with respect to the initial charged molecular species. In particular, the formation of an O^- ion and a peroxyl group by O_2^- dissociation is endothermic by 1.8–2.8 eV. In the case of O_2^{2-} dissociation, the reaction products raise the energy by an amount ranging between 1.0 and 1.7 eV. Again, we observe that structural disorder of the oxide is responsible for the finite range of values [70]. Moreover, we note that the greater the amount of negative charge carried by the molecular species, the lower the dissociation barrier and the energy of the reaction products. These results suggest that the dissociation of molecular species is favoured by a sequential capture of electrons.

4. Oxidation reaction at the Si(100)–SiO_2 interface

Recently, we addressed the oxidation reaction at the Si(100)–SiO_2 interface by using a constrained first-principles molecular dynamics approach [42]. In this study, we used three model structures of the Si(100)–SiO_2 interface, consistent with a variety of experimental data [71–73]. We obtained pathways and energy profiles for the O_2 oxidation reaction using the method described in section 3.2. In particular, during the molecular dynamics simulations we favoured the course of the oxidation reaction along an appropriate reaction coordinate by applying an external potential. Using this procedure we generated, for each model interface, 15 different reaction pathways for the O_2 molecule in both the triplet and the singlet spin state, in the neutral charge state and in the presence of one or two excess electrons. In the following, we summarize the main results obtained in this study [42].

The lowest-energy electronic configuration of the O_2 molecule in both the vacuum and the interstitials of the oxide corresponds to a triplet spin state [37, 33]. Hence, we started our simulations by locating the O_2 molecule in the triplet spin state on top of the oxide component, at the oxide–vacuum interface. We then favoured the course of the oxidation reaction by gradually decreasing the distance between the O_2 molecule and the Si(100)–SiO_2 interface. Our simulations show that the O_2 molecule approaches the interface by diffusing through neighbouring interstices (figure 7, panel A) [37]. In the proximity of the Si(100)–SiO_2 interface, the O_2 molecule attacks a Si atom in an intermediate oxidation state and incorporates in the corresponding Si–Si bond near the Si substrate (figure 7, panel B). Our simulations show that network incorporation corresponds to an exothermic process with an energy release ranging between 1.0 and 1.5 eV and proceeds by crossing energy barriers of only 0.1–0.2 eV.

Network incorporation of the O_2 molecule in the triplet spin state gives rise to network O_2 species ranging from the peroxyl linkage to a non-bridging O_2 complex accompanied by a Si

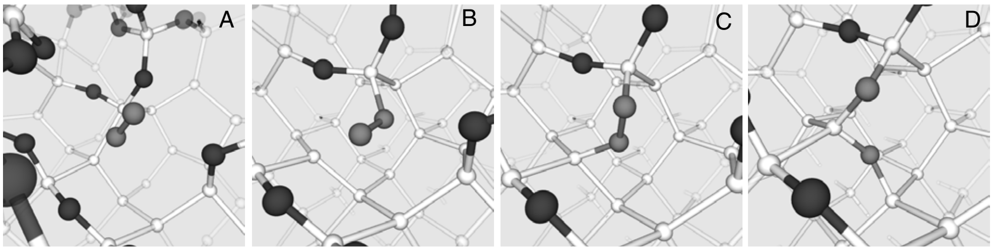

Figure 7. A neutral O_2 molecule in the triplet spin state (A) diffusing through the oxide and (B) incorporating in a Si–Si bond. The spin conversion to the singlet state is energetically favourable and drives the O_2 molecule towards the formation of a nearly symmetric peroxyl linkage (C). Dissociation of this network O_2 species gives two neighbouring Si–O–Si units (D). Light (dark) spheres relate to Si (O) atoms of the oxide network. O atoms belonging to the oxygen molecule are highlighted by grey spheres.

dangling bond (figure 7, panel B). These structures all correspond to metastable states. In fact, our electronic structure calculations show that spin conversion to the singlet spin state always lowers the energy, with energy gains ranging between 0.1 and 1.0 eV. Furthermore, upon spin conversion the atomic structure generally undergoes an important relaxation favouring the formation of a more symmetric peroxyl linkage (figure 7, panel C).

To further investigate the role of spin, we repeated our set of 15 simulations setting the O_2 molecule in the spin singlet state from the outset, while keeping otherwise identical conditions. In this case, the trajectories of the molecule through the oxide are very similar to those followed by the O_2 molecule in the triplet spin state and the incorporation in the Si–Si bond directly gives a symmetric peroxyl linkage (figure 7, panel C). Also the energetic profile is very similar to that in the triplet spin case. Hence, regardless of the spin carried by the O_2 molecule, the oxidation reaction proceeds through barriers that can easily be overcome under the usual thermal conditions of silicon oxidation [6] and results in the formation of a peroxyl linkage.

To further investigate the oxidation reaction, we favoured the dissociation of the network molecular species by taking the bond length of the molecule as the new reaction coordinate. The dynamics was constrained until the transition barrier was overcome and evolved freely afterwards. We observed that the network O_2 species dissociates by having one of the O atoms oxidize a neighbouring Si–Si bond. For our set of 15 simulations, we found transition barriers of at most 0.4 eV. These barriers are noticeably smaller than the energy released during the incorporation of the O_2 molecule, suggesting that the dissociation proceeds readily. The uptake of oxygen at the interface finally results in two neighbouring Si–O–Si units (figure 7, panel D).

To account for the occurrence of electron tunnelling processes in the vicinity of the Si substrate, we extended our investigation to the case of the O_2 molecule at the interface with either one or two excess electrons in the simulation cell [42]. Our simulations show that the availability of excess negative charge leads to a spontaneous incorporation of the O_2 molecule in the network. The incorporation of the molecule occurs through the attachment of either one or both of its O atoms to Si atoms of the oxide, which thus become fivefold coordinated. These observations are consistent with our results on the negatively charged oxygen species in a-SiO_2 (section 3.1). For both charge states considered here, the energy released upon incorporation ranges between 2 and 4 eV. This energy value is sufficiently large for overcoming the largest transition barrier (1.0 eV) associated with the ensuing dissociation. Overall, these results suggest that the availability of additional electrons further favours the course of the O_2 oxidation reaction at the Si(100)–SiO_2 interface.

5. Discussion

Our study of the kinetic processes occurring during silicon oxidation is consistent with a thick oxide regime governed by the process of O_2 diffusion through the oxide layer. Our results show that the O_2 molecule percolates through the oxide network by hopping between neighbouring interstitials. During diffusion, the O_2 molecule visits energies well below those of other neutral network oxygen species. Overall, our results [34, 37, 43, 38] are consistent with a variety of experimental [6, 10–12, 15, 16] and theoretical data [29–33, 35, 36], thereby corroborating the affirmed general understanding of the growth kinetics of thick oxide layers.

The fundamental mechanisms occurring during the growth of thin oxide layers are far less understood [6, 9, 13]. In contrast with the Deal and Grove model [6] and many other kinetics schemes [17–23], our study provides strong evidence against an activated O_2 reaction at the interface which severely influences the kinetics of the oxidation process. In fact, regardless of either the spin or the charge state, the O_2 molecule incorporates in the network at the Si(100)–SiO_2 interface by crossing energy barriers smaller than 0.2 eV [42]. Network incorporation provides energy gains ranging between 2.0 and 5.0 eV, sufficiently larger than the highest energy barrier required to complete the oxidation reaction. These results suggest that, at temperatures typically used during thermal oxidation ($\sim$1000 K), the O_2 molecule readily oxidizes Si–Si bonds at the Si(100)–SiO_2 interface. Therefore, our results favour kinetics schemes for the silicon oxidation process that are fully based on diffusive phenomena across the oxide layer [14, 24].

Kinetics models based on diffusion require a decrease of the diffusion rate near the interface to match experimental data [14]. For the neutral O_2 molecule, such an effect could be attributed to the occurrence of a thin interfacial oxide layer of higher density [44, 45]. Indeed, for oxide films thicker than 2 nm a thin densified oxide layer in contact with the Si substrate quenches percolation phenomena and reduces the diffusion rate to values below that in bulk a-SiO_2 [43, 38]. We note however that kinetics pictures based on a single molecular oxidizing species are consistent neither with the evidence of O exchange processes in the vicinity of the Si–SiO_2 interface [15, 16] nor with the observed dependence of kinetics data on pressure [6, 9, 13]. In fact, these experimental observations suggest that, in the proximity of the interface, the O_2 molecule transforms either partially or completely into a network oxygen species. For instance, the O_2 molecule approaching the interface could incorporate in Si–Si bonds well separated from the substrate. According to our results, this process occurs by crossing small energy barriers and leads to the formation of peroxyl linkages. Alternatively, the O_2 molecule may capture one or two electrons [36], giving rise to O_2^- or O_2^{2-} species. In both situations, the resulting oxygen species correspond to network defects with diffusion rates smaller than that of the neutral O_2 molecule in a-SiO_2 (see section 3.2 and [29, 32]). At the interface, these species oxidize Si–Si bonds by crossing energy barriers smaller than 0.4 eV [42]. Alternatively, the peroxyl linkage and the O_2^- and O_2^{2-} species could ultimately give rise to O^{2-} species upon further capture of electrons from the Si substrate. The latter species diffuses and oxidizes Si–Si bonds by crossing barriers of about 0.2 eV [39].

In conclusion, our findings support kinetics models of the silicon oxidation process fully governed by diffusion. Indeed, our results suggest that the oxidation of Si–Si bonds at the Si(100)–SiO_2 interface occurs by crossing small energy barriers, regardless of the nature of the oxidizing species. Moreover, our findings are consistent with a thin-film regime in which various oxygen species concomitantly participate to the oxidation process.

Acknowledgments

We thank A M Stoneham for valuable comments. We acknowledge support from the Swiss National Science Foundation (Grant No 620-57850.99). The calculations were performed at the Swiss Centre for Scientific Computing (CSCS).

References

[1] Feldman L C, Gusev E P and Garfunkel E L 1998 *Fundamental Aspects of Ultrathin Dielectrics on Si-based Devices* ed E L Garfunkel (Dordrecht: Kluwer) p 1
[2] Muller D A, Moccio S, Baumann F H, Evans-Lutterodt K and Timp G 1999 *Nature* **399** 758
[3] Green M L, Gusev E P, Degraeve R and Garfunkel E L 2001 *J. Appl. Phys.* **90** 2057
[4] Schulz M 1999 *Nature* **399** 729
[5] Wang J, Roman P, Kamieniecki E and Ruzyllo J 2003 *Electrochem. Solid-State Lett.* **6** G63
[6] Deal B E and Grove A S 1965 *J. Appl. Phys.* **36** 3770
[7] Ghez R and van der Meulen Y J 1972 *J. Electrochem. Soc.* **119** 1100
[8] Hopper M A, Clarke R A and Young L 1975 *J. Electrochem. Soc.* **122** 1216
[9] Massoud H Z, Plummer J D and Irene E A 1985 *J. Electrochem. Soc.* **132** 1745
[10] Norton F J 1961 *Nature* **191** 701
[11] Gusev E P, Lu H C, Gustafsson T and Garfunkel E L 1995 *Phys. Rev.* B **52** 1759
[12] Rosencher E, Straboni A, Rigo S and Amsel G 1979 *Appl. Phys. Lett.* **34** 254
[13] Yasuda T, Kumagai N, Nishizawa M, Yamasaki S, Oheda H and Yamabe K 2003 *Phys. Rev.* B **67** 195338
[14] Mott N F, Rigo S, Rochet F and Stoneham A M 1989 *Phil. Mag.* B **60** 189
[15] Åkermark T, Gosset L G, Ganem J J, Trimaille I and Rigo S 1999 *J. Electrochem. Soc.* **146** 3389
[16] Åkermark T, Ganem J J, Trimaille I, Vickridge I and Rigo S 1999 *J. Phys. Chem.* B **103** 9910
[17] Verdi L and Miotello A 1995 *Phys. Rev.* B **51** 5469
[18] Dimitrijev S and Harrison H B 1996 *J. Appl. Phys.* **80** 2467
[19] Stockhausen A, Kampen T U and Mönch W 1992 *Appl. Surf. Sci.* **56** 795
[20] Westermann J, Nienhaus H and Mönch W 1994 *Surf. Sci.* **311** 101
[21] Peng K Y, Wang L C and Slattery J C 1996 *J. Vac. Sci. Technol.* B **14** 3316
[22] Wolters D R and Zengers van Duijnhoven A T A 1998 *Microelectron. Reliab.* **38** 259
[23] de Almeida R M C, Gonçalves S, Baumvol I J R and Stedile F C 2000 *Phys. Rev.* B **61** 12992
[24] Doremus R H and Szewczyk A 1987 *J. Mater. Sci.* **22** 2887
[25] Pasquarello A, Hybertsen M S and Car R 1998 *Nature* **396** 58
[26] Stefanov B B and Raghavachari K 1997 *Surf. Sci.* **389** L1159
[27] Kato K, Uda T and Terakura K 1998 *Phys. Rev. Lett.* **80** 2000
[28] Tu Y and Tersoff J 2002 *Phys. Rev. Lett.* **89** 086102
[29] Hamann D R 1998 *Phys. Rev. Lett.* **81** 3447
[30] Szymanski M A, Stoneham A M and Shluger A L 2000 *Microelectron. Reliab.* **40** 567
[31] Chelikowsky J R, Chadi D J and Binggeli N 2000 *Phys. Rev.* B **62** 2251
[32] Roma G, Limoge Y and Baroni S 2001 *Phys. Rev. Lett.* **86** 4564
[33] Orellana W, da Silva A J R and Fazzio A 2001 *Phys. Rev. Lett.* **87** 155901
[34] Bongiorno A and Pasquarello A 2001 *Microelectron. Reliab.* **59** 167
[35] Bakos T, Rashkeev S N and Pantelides S T 2002 *Phys. Rev. Lett.* **88** 55508
[36] Stoneham A M, Szymanski M A and Shluger A L 2001 *Phys. Rev.* B **63** R241304
[37] Bongiorno A and Pasquarello A 2002 *Phys. Rev. Lett.* **88** 125901
[38] Bongiorno A and Pasquarello A 2004 *Phys. Rev.* B **70** 195312
[39] Jin Y and Chang K J 2001 *Phys. Rev. Lett.* **86** 1793
[40] Orellana W, da Silva A J R and Fazzio A 2003 *Phys. Rev. Lett.* **90** 16103
[41] Akiyama T and Kageshima H 2003 *Appl. Surf. Sci.* **216** 270
[42] Bongiorno A and Pasquarello A 2004 *Phys. Rev. Lett.* **93** 86102
[43] Bongiorno A and Pasquarello A 2003 *J. Phys.: Condens. Matter* **15** S1553
[44] Awaji N, Ohkubo S, Nakanishi T, Sugita Y, Takasaki K and Komiya S 1996 *Japan. J. Appl. Phys.* **35** L67
[45] Kosowsky S D, Pershan P S, Krish K S, Bevk J, Green M L, Brasen D, Feldman L C and Roy P K 1997 *Appl. Phys. Lett.* **70** 3119
[46] van Beest B W H, Kramer G J and van Santen R A 1990 *Phys. Rev. Lett.* **64** 1955
[47] Devine R A B, Capponi J J and Arndt J 1987 *Phys. Rev.* B **35** 770
[48] Rochet F, Agius B and Rigo S 1984 *J. Electrochem. Soc.* **131** 914
[49] Rochet F, Rigo S, Froment M, d'Anterroches C, Maillot C, Roulet H and Dufour G 1986 *Adv. Phys.* **35** 237
[50] Trimaille I and Rigo S 1989 *Appl. Surf. Sci.* **39** 65
[51] Costello J A and Tressler R E 1984 *J. Electrochem. Soc.* **131** 1944
[52] Afanas'ev V V 1999 *Microelectron. Eng.* **48** 241
[53] Jorgensen P J 1962 *J. Chem. Phys.* **37** 874
[54] Raleigh D O 1966 *J. Electrochem. Soc.* **113** 782

[55] Jorgensen P J 1967 *J. Electrochem. Soc.* **114** 820
[56] Raleigh D O 1968 *J. Electrochem. Soc.* **115** 111
[57] Modlin D N and Tiller W A 1985 *J. Electrochem. Soc.* **132** 1659
[58] Hohenberg P and Kohn W 1964 *Phys. Rev.* **9** B864
[59] Kohn W and Sham L J 1965 *Phys. Rev.* **15** A1133
[60] Perdew J P, Chevary J A, Vosko S H, Jackson K A, Pederson M R, Singh D J and Fiolhais C 1992 *Phys. Rev.* B **46** 6671
[61] Dal Corso A, Pasquarello A, Baldereschi A and Car R 1996 *Phys. Rev.* B **53** 1180
[62] Vanderbilt D 1990 *Phys. Rev.* B **41** 7892
[63] Pasquarello A, Laasonen K, Car R, Lee C and Vanderbilt D 1992 *Phys. Rev. Lett.* **69** 1982
[64] Laasonen K, Pasquarello A, Car R, Lee C and Vanderbilt D 1993 *Phys. Rev.* B **47** 10142
[65] Markov G and Payne M C 1995 *Phys. Rev.* B **51** 4014
[66] Harris F E and Monkhorst H J 1969 *Phys. Rev.* B **2** 4400
[67] Tassone F, Mauri F and Car R 1994 *Phys. Rev.* B **50** 10561
[68] Barkema G T and Mousseau N 1996 *Phys. Rev. Lett.* **77** 4358
[69] Lide D R and Frederikse H P R (ed) 1998 *CRC Handbook of Chemistry and Physics* (New York: Chemical Rubber Company Press)
[70] Szymanski M A, Shluger A L and Stoneham A M 2001 *Phys. Rev.* B **63** 224207
[71] Bongiorno A and Pasquarello A 2003 *Appl. Phys. Lett.* **83** 1417
[72] Bongiorno A, Pasquarello A, Hybertsen M S and Feldman L C 2003 *Phys. Rev. Lett.* **90** 186101
[73] Bongiorno A and Pasquarello A 2004 *Appl. Surf. Sci.* **234** 190